Development of an Aerosol Opacity Retrieval Algorithm for use with Multi-angle Land Surface Images

David J. Diner, Susan R. Paradise, and John V. Martonchik
Jet Propulsion Laboratory, California Institute of Technology
Mail Stop 169-237
4800 Oak Grove Drive
Pasadena, CA 91109 USA
T: 818.354.6319 F: 818.393.4619 EMail: djd@jord.jpl.nasa.gov
T: 818.354.2112 F: 818.393.4619 EMail: srp@jord.jpl.nasa.gov
T: 818.354.2207 F: 818.393.4619 EMail: jvm@jord.jpl.nasa.gov

ABSRACT

In 1998, the Multi-angle Imaging SpectroRadiometer (MISR) will fly aboard the EOS-AM1 spacecraft. MISR will enable unique methods for retrieving the properties of atmospheric aerosols, by providing global imagery of the Earth at nine viewing angles in four visible and near-IR spectral bands. As part of the MISR algorithm development, theoretical methods of analyzing multi-angle, multi-spectral data are being tested using images acquired by the airborne Advanced Solid-State Array Spectroradiometer (ASAS). In this paper we derive a method to be used over land surfaces for retrieving the change in opacity between spectral bands, which can then be used in conjunction with an aerosol model to derive a bound on absolute opacity. We demonstrate the method using ASAS data.

INTRODUCTION

MISR (Diner et al., 1993) will be launched into polar orbit on the Earth Observing System (EOS) AM1 spacecraft in June 1998. It contains nine push-broom cameras to observe at fixed view angles, relative to the surface normal, of 0° (nadir), and 26.1°, 45.6°, 60.0°, and 70.5° fore and aft of nadir using charge-coupled device line arrays filtered to 443, 555, 670, and 865 nm. The camera focal lengths provide 275-m crosstrack footprints at all off-nadir angles (250 m in the nadir). Along-track sample spacing is 275 m at all angles. The swath seen in common by all cameras is 360 km wide.

Aerosol studies are among the objectives of the MISR experiment. We are using the airborne ASAS instrument (Irons et al., 1991) for development and validation of MISR algorithms. ASAS acquires multi-angle push-broom images in contiguous spectral bands; the data discussed here cover the spectral range 462 to 866 nm. The crosstrack swath width is 1.7 km at a flight altitude of 5 km, and the ground sample spacing is 3.3 m at nadir. Aboard the C-130 aircraft, the ASAS tilt mechanism allows data to be taken at angles relative to the surface normal ranging from 70° forward to 55° aftward.

The algorithm described in this paper provides constraints which will then be used as inputs to other steps in the aerosol retrieval process (Martonchik and Conel, 1994). We take advantage of the applicability of 3-D radiative transfer theory at sub-kilometer resolution. Over regions of heterogeneous reflectance, only that component of the observed radiance field which corresponds to directly transmitted surface-leaving radiances contains spatial contrasts. That is, over these spatial scales diffusely scattered upwelling radiation will be horizontally uniform. If the surface properties at two wavelengths are highly correlated, we can then derive an expression that is largely independent of the surface properties and dependent primarily on the spectral difference in optical depth, $\Delta\tau$, which can be determined from multi-angle views.

THEORY

The observed multi-angle radiance L can be written as

$$L_{x,y}(-\mu, \mu_0, \phi-\phi_0) = L^{atm}(-\mu, \mu_0, \phi-\phi_0) + \exp(-\tau/\mu) \times \frac{1}{\pi}\int_0^{2\pi}\int_0^{1} R^{surf}_{x,y}(-\mu, \mu', \phi-\phi') L^{inc}(\mu', \mu_0, \phi'-\phi_0)\, \mu' d\mu' d\phi' + \frac{1}{\pi}\int_0^{2\pi}\int_0^{1}\int_0^{2\pi}\int_0^{1} T_{x,y}(-\mu, -\mu'', \phi-\phi'') \otimes R^{surf}_{x,y}(-\mu'', \mu', \phi''-\phi') L^{inc}(\mu', \mu_0, \phi'-\phi_0)\, \mu' d\mu'' d\phi'' d\mu' d\phi' \quad (1)$$

where x, y are spatial coordinates, μ and μ_0 are the view and solar zenith angle cosines, and $\phi-\phi_0$ is the view azimuthal angle relative to the Sun. The convention -μ and μ is used for upwelling and downwelling radiation respectively. The atmosphere is assumed to be horizontally homogeneous. L^{atm} is the diffuse path radiance, τ is the optical depth, L^{inc} is the direct and diffuse radiance field incident on the surface (assumed to be horizontally uniform), T is the upward diffuse transmittance, and R^{surf} is the spatially variable surface bidirectional reflectance factor. The transmittance T can be thought of as a point-spread function and with the convolution operation $\otimes$ describes the blurring effect of the atmosphere on R^{surf} (Diner and Martonchik, 1985). We now define the surface hemispherical directional reflectance factor, r:

$$r_{x,y}(-\mu, \mu_0, \phi-\phi_0) = \frac{1}{\pi E(\mu_0)}\int_0^{2\pi}\int_0^{1} R^{surf}_{x,y}(-\mu, \mu', \phi-\phi') L^{inc}(\mu', \mu_0, \phi'-\phi_0)\, \mu' d\mu' d\phi' \quad (2)$$

where E is the surface irradiance. Finally, we define the top-of-atmosphere bidirectional reflectance factor R by $R = \pi L / (\mu_0 E_0)$, where E_0 is the exo-atmospheric solar irradiance. Now, at sub-kilometer resolution the first and third terms on the right-hand-side of Eq. (1) are nearly spatially uniform. Taking differences of adjacent pixels in the crosstrack direction and using Eq. (2):

$$R_{x,y+1}(\mu, \mu_0, \phi-\phi_0) - R_{x,y}(\mu, \mu_0, \phi-\phi_0) = \hat{R}_{x,y}(\mu, \mu_0, \phi-\phi_0) = \frac{\pi E(\mu_0)}{\mu_0 E_0}\hat{r}_{x,y}(-\mu, \mu_0, \phi-\phi_0)\exp(-\tau/\mu) \quad (3)$$

where the caretted symbols indicate pixel differences. Considering Eq. (3) at two wavelengths, λ and λ_0, and taking the ratio, we have

0-7803-1497-2/94 $4.00 © 1994 IEEE

$$\frac{\hat{R}_{x,y,\lambda}}{\hat{R}_{x,y,\lambda_0}} = \exp(-\Delta\tau/\mu) \cdot \frac{[E(\mu_0)/E_0]_\lambda}{[E(\mu_0)/E_0]_{\lambda_0}} \cdot \frac{\hat{r}_{x,y,\lambda}(-\mu, \mu_0, \phi-\phi_0)}{\hat{r}_{x,y,\lambda_0}(-\mu, \mu_0, \phi-\phi_0)} \quad (4)$$

where $\Delta\tau = \tau(\lambda) - \tau(\lambda_0)$. If the surface reflectances (both angular shape and spatial pattern) are highly correlated, the ratio of the reflectance factor fields can be modelled as a constant, independent of spatial location and view angle, in which case Eq. (4) simplifies to

$$\hat{R}_{x,y,\lambda} = a \cdot \exp(-\Delta\tau/\mu)\, \hat{R}_{x,y,\lambda_0} \quad (5)$$

Hence, $a \cdot \exp(-\Delta\tau/\mu)$ is the slope, s, of the line formed by plotting $\hat{R}_{x,y,\lambda}$ against $\hat{R}_{x,y,\lambda_0}$. After finding s, we can solve for $\Delta\tau$, the y-intercept of the line:

$$-\mu \ln(s) = \Delta\tau - \mu \ln(a) \quad (6)$$

ANALYSIS

The primary ASAS data set used in this analysis was taken on February 26, 1992 at Glacier National Park, Montana, over snow-covered Bowman Lake, surrounded by pine trees, at 48.83° North latitude and 114.19° West longitude, and an altitude of 1.250 km. The solar zenith angle was 63.4°, and the azimuth was 214.1°. The airplane flew at an altitude of 4.450 km, heading 234.63° from true North. The 559.4 nm image acquired at 30° forward of nadir is shown in Fig. 1. Images were also acquired at nadir, 15, 45, 60, and 70° forward of nadir and 15, 30, 45, and 55° aftward of nadir.

Figure 1. Glacier image at 559.4 nm and 30° forward of nadir

The 256 x 256 pixel data set was averaged to 32 x 32 pixels for the analysis in order to improve the signal-to-noise ratio. Then, difference images were formed by taking differences of adjacent pixels in the cross-track direction. Figure 2 shows the correlation between the 462.0 nm differenced nadir image and the 559.4 nm differenced nadir image, as a test of Eq. (5). A high degree of linear correlation is observed.

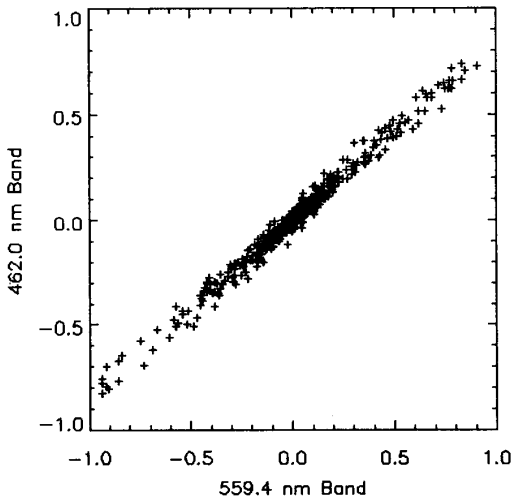

Figure 2. Correlation between differenced nadir images at 462.0 nm and 559.4 nm

The cross correlation coefficient, which is the ratio of the square of the covariance of the two data sets divided by the product of their variances, is shown at each view angle as a function of wavelength in Fig. 3, using 559.4 nm as the reference wavelength (λ_0). Note that beyond about 700 nm the correlations deteriorate dramatically. This is due to the large change in vegetation reflectance from the visible to the near-IR. Similar correlations as shown in Fig. 2, and the loss of correlation beyond 700 nm are observed in other ASAS data sets, for example, imagery of cotton fields and bare soil acquired over Maricopa, Arizona on September 7, 1991. Because of the limited view angle range of the Maricopa data (±45°), they are not suitable for spectral optical depth retrieval; nevertheless they substantiate the existence of the correlations which are fundamental to the method.

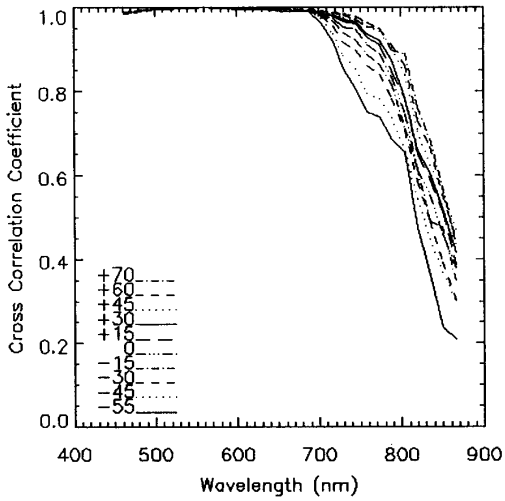

Figure 3. Cross correlation coefficient for the10 view angles as a function of wavelength

The slope s of the spectral correlations (e.g., Fig. 2) is then found at all view angles and wavelengths. Figure 4 shows $-\mu \ln(s)$ vs. μ for the 462.0 nm and 559.4 nm bands of the Glacier data set.

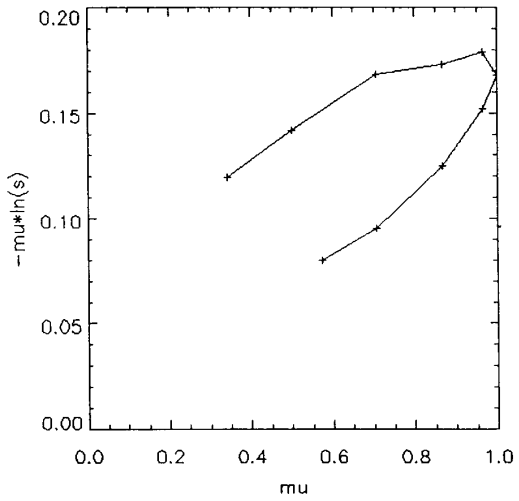

Figure 4. Test of Eq. (6) for 463.0 nm data correlated with 559.4 nm data at all view angles

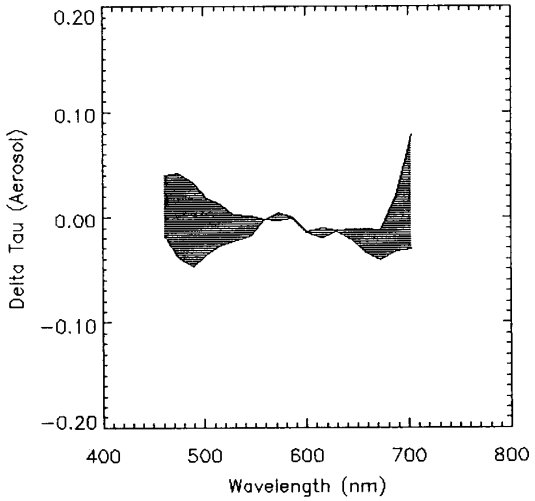

Figure 5. Upper and lower bounds on $\Delta\tau_{aerosol}$ vs. wavelength

We find that the relation is not exactly linear, as predicted by Eq. (6), and also shows some difference between the forward and aftward views. This leads us to conclude that the assumption made in Eq. (5), that the ratio of the surface reflectances from the two different wavelengths is a constant, is not strictly true. To account for this, suppose that instead of being a constant, the ratio of the reflectances were a low-order polynomial in μ, $P(\mu)$, again independent of spatial position. Then Eq. (6) becomes:

$$-\mu \ln(s) = \Delta\tau - \mu \ln[P(\mu)] \quad (7)$$

with the right-hand side approaching $\Delta\tau$ as $\mu \rightarrow 0$. Then Eq. (7) should become more linear for μ close to 0. Therefore, instead of fitting a single straight line simultaneously to both branches of the curves shown in Fig. 4, we fit a straight line to the data at the two highest view angles (i.e., smallest values of μ), independently for the forward and aftward branches. These extrapolations provide upper and lower bounds on $\Delta\tau$ and we interpret the difference as a measure of the uncertainty in $\Delta\tau$ that can be derived using this approach.

RESULTS

Using the Glacier data, $\Delta\tau_{aerosol}$ was retrieved over the range 450 to 700 nm, as shown in Fig. 5. The reference wavelength is 559.4 nm. Values for $\Delta\tau_{aerosol}$ were determined by retrieving the total column spectral optical depth difference, given by $\Delta\tau_{aerosol} + \Delta\tau_{Rayleigh}$, then subtracting the Rayleigh contribution which was calculated using its well-known spectral dependence, assuming a standard atmosphere, and taking into account the terrain and aircraft altitudes. The small values of $\Delta\tau_{aerosol}$ indicate either that the aerosol is spectrally "gray", or that its optical depth is spectrally variable and its absolute optical depth is low. The "continental" aerosol expected in this geographic location exhibits approximately a λ^{-2} dependence in its optical depth (d'Almeida et al., 1991), from which we derive a mean upper bound of 0.076 for the absolute aerosol optical depth at 559.4 nm. This result is consistent with an upper bound derived by an independent method making use of the darkest pixels in the image. Since the method described here constrains the abundance and type of aerosol (although not both independently) we plan to use it as one step in the operational aerosol retrievals to be performed over land with MISR.

ACKNOWLEDGMENTS

We thank J. Irons and D. Hall of the Goddard Space Flight Center for providing the ASAS imagery used in this analysis and L. Barge and B. Rheingans for geometrically rectifying and registering the images. This research was performed by the Jet Propulsion Laboratory, California Institute of Technology, under contract with the National Aeronautics and Space Administration.

REFERENCES

d'Almeida, G. A., P. Koepke, and E. P. Shettle. *Atmospheric Aerosols: Global climatology and radiative characteristics.* Deepak Publishing, 1991.

Diner, D. J. and J. V. Martonchik. "Influence of aerosol scattering on atmospheric blurring of surface features." *IEEE Trans. Geosci. and Rem. Sens.* 23 (1985): 618-624.

Diner, D.J., C.J. Bruegge, T. Deslis, V.G. Ford, L.E. Hovland, D.J. Preston, M.J. Shterenberg, E.B Villegas, and M.L. White. "Development status of the EOS Multi-angle Imaging SpectroRadiometer (MISR)." *SPIE Proc.* 1939 (1993): 94-103.

Irons, J.R., K.J. Ranson, D.L. Williams, R.R. Irish, and F.G. Huegel. "An off-nadir-pointing imaging spectroradiometer for terrestrial ecosystem studies." *IEEE. Trans. Geosci. Rem. Sens.* 29 (1991): 66-74.

Martonchik, J. V. and J. E. Conel. "Retrieval of surface reflectance and atmospheric properties using ASAS imagery," in *IGARSS'94 Symposium*, 1994, this session.